A Split-Step Scheme for the Incompressible Navier-Stokes Equations

William D. Henshaw and N. Anders Petersson

Centre for Applied Scientific Computing,
Lawrence Livermore National Laboratory,
Livermore, CA, 94551,
henshaw@llnl.gov, andersp@llnl.gov

October 29, 2001

Abstract. We describe a split-step finite-difference scheme for solving the incompressible Navier-Stokes equations on composite overlapping grids. The split-step approach decouples the solution of the velocity variables from the solution of the pressure. The scheme is based on the velocity-pressure formulation and uses a method of lines approach so that a variety of implicit or explicit time stepping schemes can be used once the equations have been discretized in space. We have implemented both second-order and fourth-order accurate spatial approximations that can be used with implicit or explicit time stepping methods. We describe how to choose appropriate boundary conditions for the pressure to make the scheme accurate and stable. A divergence damping term is added to the pressure equation to keep the numerical dilatation small. Several numerical examples are presented.

1 Introduction

We consider solving the incompressible Navier-Stokes equations with finite difference methods on composite overlapping grids using an accurate and stable split-step approach that decouples the solution of the velocity from the solution of the pressure. Second-order and fourth-order accuracy has been achieved in space and second or higher order accuracy in time can be easily accomplished.

In primitive-variables the initial-boundary-value problem (IBVP) for the incompressible Navier-Stokes equations is

$$
\begin{aligned}
\partial \mathbf{u}/\partial t + (\mathbf{u}\cdot\nabla)\mathbf{u} + \nabla p &= \nu \Delta \mathbf{u} + \mathbf{F}, && \text{for } \mathbf{x}\in\Omega, \quad t>0,\\
\nabla\cdot\mathbf{u} &= 0, && \text{for } \mathbf{x}\in\overline{\Omega}, \quad t>0,\\
B(\mathbf{u},p) &= \mathbf{g}, && \text{for } \mathbf{x}\in\partial\Omega, \ t>0,\\
\mathbf{u}(\mathbf{x},0) &= \mathbf{f}(\mathbf{x}), && \text{for } \mathbf{x}\in\Omega.
\end{aligned}
\tag{1}
$$

Here $\mathbf{u}=(u_1,u_2,u_3)$ is the velocity, p is the kinematic pressure (pressure divided by the constant density), ν is the kinematic viscosity, $\mathbf{F}$ is the forcing per unit volume, Ω is a bounded open domain in R^d, $d=2$ or $d=3$, and $\partial\Omega$ is the boundary of Ω. The initial conditions should satisfy $\nabla\cdot\mathbf{f}=0$. There are d boundary conditions denoted by $B(\mathbf{u},p)=0$. On a fixed wall, for example, the boundary conditions are $\mathbf{u}=0$. We assume that all data are sufficiently smooth and compatible. Depending on the boundary conditions the pressure may only be determined up to a constant in which case we impose the average pressure to be zero. We refer to the formulation (1) as the "velocity-divergence" formulation.

An alternative form of this IBVP, which we call the "velocity-pressure" formulation, is

$$\begin{aligned}
\partial \mathbf{u}/\partial t + (\mathbf{u}\cdot\nabla)\mathbf{u} + \nabla p &= \nu \Delta \mathbf{u} + \mathbf{F}, && \text{for } \mathbf{x}\in\Omega, \quad t>0, \\
\Delta p + J(\nabla\mathbf{u}) - \alpha(\mathbf{x})\nabla\cdot\mathbf{u} &= \nabla\cdot\mathbf{F}, && \text{for } \mathbf{x}\in\Omega, \quad t\geq 0, \\
B(\mathbf{u},p) &= \mathbf{g}, && \text{for } \mathbf{x}\in\partial\Omega, \ t>0, \\
\nabla\cdot\mathbf{u} &= 0, && \text{for } \mathbf{x}\in\partial\Omega, \\
\mathbf{u}(\mathbf{x},0) &= \mathbf{f}(\mathbf{x}), && \text{for } \mathbf{x}\in\Omega,
\end{aligned} \tag{2}$$

where

$$J(\nabla\mathbf{u}) = \sum_{m=1}^{d} \nabla u_m \cdot \frac{\partial \mathbf{u}}{\partial x_m}.$$

Here, the equation $\nabla\cdot\mathbf{u}=0$ in (1) has been replaced by an elliptic equation for the pressure, which is obtained by taking the divergence of the momentum equations, and using $\nabla\cdot\mathbf{u}=0$. The Poisson equation for the pressure needs an additional boundary condition and the boundary condition on the dilatation in (2) fills this purpose. Although $\nabla\cdot\mathbf{u}=0$ does not look like a boundary condition for p, once the equations have been discretized the connection will become apparent. We have also added the **divergence damping** term,

$$\alpha(\mathbf{x})\nabla\cdot\mathbf{u}\ , \qquad \alpha\geq 0\ ,$$

to the pressure equation. In the continuous case this term has no effect, but in the discrete case this term will be important to keep the dilatation small. To see why this term might be important we can write down the equation satisfied by the dilatation, $\delta=\nabla\cdot\mathbf{u}$, formed by taking the divergence of the momentum equation,

$$\partial\delta/\partial t + (\mathbf{u}\cdot\nabla)\delta = \nu\Delta\delta - \alpha\delta. \tag{3}$$

The term we have added to the pressure equation appears as a linear damping term in the evolution equation for the divergence. Note that $\delta(\mathbf{x},t)$ will be identically zero for all times since the initial condition is $\delta(\mathbf{x},0)=0$ and the boundary condition is $\delta(\mathbf{x},t)=0$. This observation motivates the extra boundary condition $\nabla\cdot\mathbf{u}=0$, since it forces the dilatation to be zero everywhere for all times and thus guarantees that solutions of the velocity-pressure system (2) also satisfy the velocity-divergence equations (1).

The incompressible Navier-Stokes equations in primitive variables can be discretized in a variety of ways. Harlow and Welch [8] provided what was perhaps the first discretization with the MAC technique using staggered grids. Later the projection method was devised by Chorin[5] and independently by Temam[25]. The projection method was extended to an implicit fractional-step

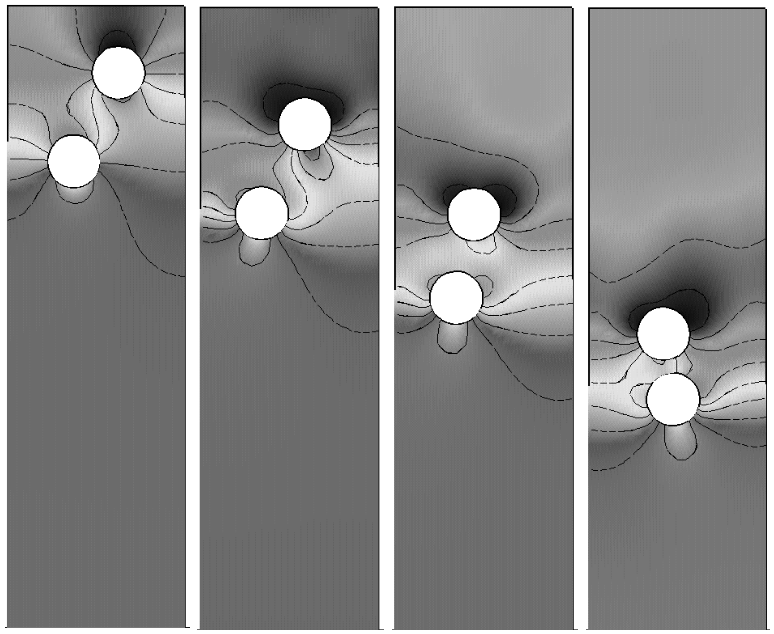

Fig. 1. Two falling bodies in an incompressible flow. The overlapping grids are recomputed at every time-step.

method by Kim and Moin[15]. The method of artificial compressibility, introduced by Chorin [4], is another popular approach. For example, this method was used by Kiris et al. [16] to compute the flow in an artifical heart. There have been numerous other approaches developed based on finite-difference, finite-volume, finite-element and spectral-element discretizations, such as [1][2][14][26][17][23][9], to name a few.

There are a number of fundamental issues that must be dealt with when designing a scheme for the incompressible Navier-Stokes equations:

- The pressure should be free of spurious oscillations. Straight-forward discretizations of (1) can lead to the checker-board instability (corresponding to a violation of the Babuška-Brezzi condition in finite-elements).
- Many approaches require extra boundary conditions, either for the pressure or for an intermediate velocity field, which can be non-trivial to choose.
- If the pressure is only determined up to a constant (for example when Neumann boundary conditions are enforced on $\partial\Omega$), there will be a compatibility condition on the data for the pressure equation.
- For efficiency it is useful to decouple the solution of the velocity from the solution of the pressure.
- The discrete divergence should be small, i.e., of the order of the truncation error in the numerical method.

There have been long discussions in the literature related to these issues, especially concerning boundary conditions for the pressure [7,18,14,23] and whether fractional-step projection methods are inherently first-order accurate in the pressure [19,24,22,6]. We refer to Brown et. al. [3] for a discussion of how to get second-order accuracy in the pressure with the fractional-step projection method. In the present paper, we summarize the results of our research, and describe how the above four issues are handled in our approach.

Here we describe a straight-forward approach that leads to an efficient second (or higher) order accurate scheme in both the velocity and the pressure. We use a method of lines approach to discretize the velocity-pressure formulation (2). We begin by discretizing in space. For ease of presentation we consider solving the equations in two space dimensions on a square grid $\mathbf{G}$, with grid spacing $h = 1/N$, for N a positive integer:

$$\mathbf{G} = \{\mathbf{x_i} = (x_\mathbf{i}, y_\mathbf{i}) = (ih, jh) \qquad i, j = -1, 0, 1, \ldots, N+1\}$$

Here $\mathbf{i} = (i, j)$ is a multi-index. We include ghost points at the boundaries to aid in the discretization. To be specific, we consider a Dirichlet boundary condition for the velocity:

$$\mathbf{u}(\mathbf{x}, t) = \mathbf{g}(\mathbf{x}, t). \tag{4}$$

We first discretize in space. Let $(\mathbf{U_i}(t), P_\mathbf{i}(t))$ be the numerical approximation to $(\mathbf{u}(\mathbf{x}, t), p(\mathbf{x}, t))$ with $\mathbf{U_i}(t) = (U_\mathbf{i}(t), V_\mathbf{i}(t))$. The spatial approximation is

$$\begin{aligned}
d\mathbf{U_i}/dt &= -(\mathbf{U_i} \cdot \nabla_h)\mathbf{U_i} - \nabla_h P_\mathbf{i} + \nu \Delta_h \mathbf{U_i} + \mathbf{F_i}, && i, j = 1, 2, \ldots, N-1 && (5)\\
\Delta_h P_\mathbf{i} &= \alpha_\mathbf{i} \nabla_h \cdot \mathbf{U_i} - J(\nabla_h \mathbf{U_i}) + \nabla_h \cdot \mathbf{F_i}, && i, j = 0, 1, 2, \ldots, N && (6)\\
\mathbf{U_i} &= \mathbf{g}(\mathbf{x_i}, t) \equiv (g^u(\mathbf{x_i}, t), g^v(\mathbf{x_i}, t)) && i = 0, j = 0, 1, 2, \ldots, N && (7)\\
D_{0x} U_\mathbf{i} &= -D_{0y} g^v_\mathbf{i} && i = 0, j = 0, 1, 2, \ldots, N && (8)
\end{aligned}$$

The boundary conditions have only been specified at $x = 0$; similar expressions will hold at the other boundaries. The operators ∇_h, Δ_h are the standard centered difference approximations to ∇ and Δ:

$$\begin{aligned}
\nabla_h \cdot \mathbf{U_i} &= D_{0x}\mathbf{U_i} + D_{0y}\mathbf{U_i}\ , & \Delta_h \mathbf{U_i} &= (D_{+x}D_{-x} + D_{+y}D_{-y})\mathbf{U_i},\\
D_{0x}\mathbf{U_i} &= \frac{\mathbf{U}_{i+1,j} - \mathbf{U}_{i-1,j}}{2h}\ , & D_{0y}\mathbf{U_i} &= \frac{\mathbf{U}_{i,j+1} - \mathbf{U}_{i,j-1}}{2h},\\
D_{+x}\mathbf{U_i} &= \frac{\mathbf{U}_{i+1,j} - \mathbf{U}_{i,j}}{h}\ , & D_{-x}\mathbf{U_i} &= \frac{\mathbf{U}_{i,j} - \mathbf{U}_{i-1,j}}{h}.
\end{aligned}$$

We avoid the checker-board instability problem since we have directly discretized the pressure equation using a compact difference approximation. The discrete approximation will require extra numerical boundary conditions. Applying the general principle for deriving numerical boundary conditions described in [13], we use the equations themselves to tell how the solution should behave at the boundary. Note for example, that the pressure equation (6) is applied on the boundary, $i = 0$. As a numerical boundary condition, we could also apply the momentum equations on the boundary and thus determine the values for $\mathbf{U}_{-1,j}$. However, in order to keep the solution of the pressure decoupled from the velocity, we instead only apply the normal component of the momentum equation on the boundary,

$$\frac{\partial p}{\partial n} = \mathbf{n} \cdot (-\mathbf{g}_t - (\mathbf{g} \cdot \nabla)\mathbf{u} + \nu \Delta \mathbf{u}) , \tag{9}$$

and extrapolate the tangential component of the velocity,

$$D_{+x}^3 V_{-1j} \equiv V_{-1j} - 3V_{0j} + 3V_{1j} - V_{2j} = 0. \tag{10}$$

We call (9) the div-grad pressure boundary condition. Note that by itself it adds no new information to the continuous PDE and cannot replace $\nabla \cdot \mathbf{u} = 0$ as the extra boundary condition required by the velocity-pressure formulation. After discretization, (9) becomes

$$D_{0x} P_{0j} = \nu D_{+x} D_{-x} U_{0j}, \quad j = 0, 1, \ldots , N, \tag{11}$$

where we assumed $\mathbf{g} = 0$ for simplicity. We can now see how $\nabla \cdot \mathbf{u} = 0$ provides a boundary condition for the pressure: the discrete divergence boundary condition (8) determines the ghost line value of the normal component of the velocity, $U_{-1,j}$, which is used in (11). By eliminating that ghost line value, we obtain a special stencil for the right hand side:

$$D_{0x} P_{0j} = \nu \frac{2}{h} D_{+x} U_{0j}, \quad j = 0, 1, \ldots , N.$$

We believe that the reason (9) is not more widely used is due to the fact that applying a discrete form of (9) can easily lead to a unstable method since the second-derivative of $\mathbf{u}$ appears on the right hand side. To achieve a stable scheme using (9), it is extremely important to also enforce the essential boundary condition $\nabla \cdot \mathbf{u} = 0$.

Equations (5-8, 11, 10) can be solved with a method of lines approach. If we wish to have a split-step scheme where the solution of the pressure equation is decoupled from the solution of the velocity components, we should choose a time stepping scheme for the velocity components that only involves the pressure from previous time steps. Let us introduce the operators $L = L_E + L_I$ representing various terms in the momentum equation:

$$\begin{aligned} L\mathbf{U_i} &= -(\mathbf{U_i} \cdot \nabla_h)\mathbf{U_i} - \nabla_h P_\mathbf{i} + \nu \Delta_h \mathbf{U_i}, \\ L_E \mathbf{U_i} &\equiv -(\mathbf{U_i} \cdot \nabla_h)\mathbf{U_i} - \nabla_h P_\mathbf{i}, \\ L_I \mathbf{U_i} &\equiv \nu \Delta_h \mathbf{U_i}. \end{aligned}$$

L_I and L_E will be the parts of the operator that we treat implicitly and explicitly, respectively.

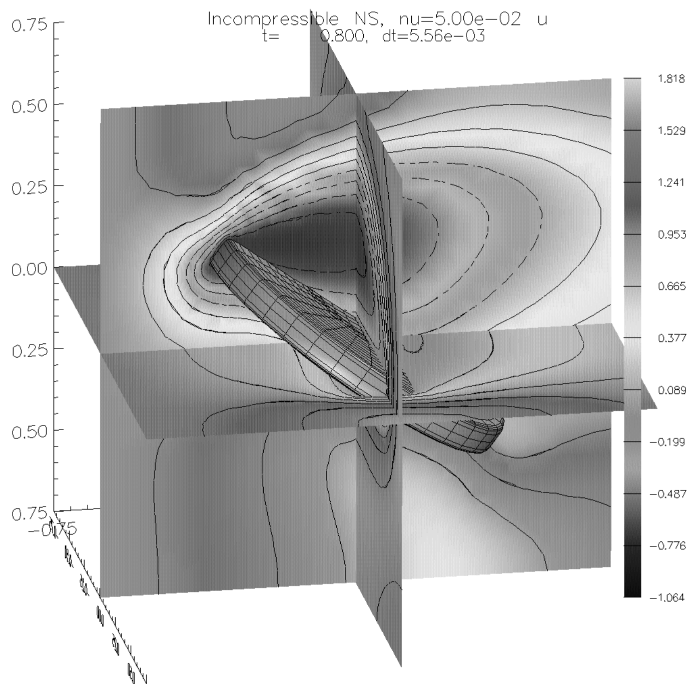

Fig. 2. Flow past a rotating disk.

1.1 An explicit scheme

As a first example we solve these equations with the explicit second-order Adams-Bashforth scheme. In this approach we first advance the velocity using

$$
\begin{aligned}
\frac{\mathbf{U}_{\mathbf{i}}^{n+1}-\mathbf{U}_{\mathbf{i}}^{n}}{\Delta t} &= \frac{3}{2}(L\mathbf{U}_{\mathbf{i}}^{n}+\mathbf{F}_{\mathbf{i}}^{n})-\frac{1}{2}(L\mathbf{U}_{\mathbf{i}}^{n-1}+\mathbf{F}_{\mathbf{i}}^{n-1}), && i,j=1,\dots,N-1, && (12)\\
\mathbf{U}_{\mathbf{i}}^{n+1} &= \mathbf{g}(\mathbf{x}_{\mathbf{i}},t^{n+1}), && i=0,j=0,\dots,N, && (13)\\
D_{0x}U_{\mathbf{i}}^{n+1} &= -D_{0y}g^{v}(\mathbf{x}_{\mathbf{i}},t^{n+1}), && i=0,j=0,\dots,N, && (14)\\
D_{+x}^{3}V_{-1j}^{n+1} &= 0, && j=0,\dots,N. && (15)
\end{aligned}
$$

Here $\mathbf{U}_{\mathbf{i}}^{n} \approx \mathbf{u}(\mathbf{x}_{\mathbf{i}}, n\Delta t)$. These equations determine $\mathbf{U}_{\mathbf{i}}^{n+1}$ at all points including the ghost points. We then solve for the pressure from

$$
\begin{aligned}
\Delta_h P_{\mathbf{i}}^{n+1} - \alpha_{\mathbf{i}}\nabla_h\cdot\mathbf{U}_{\mathbf{i}}^{n+1} + J(\nabla_h\mathbf{U}_{\mathbf{i}}^{n+1}) &= 0, && i,j=0,1,\dots,N, && (16)\\
D_{0x}P_{\mathbf{i}}^{n+1} &= \nu D_{+x}D_{-x}U_{\mathbf{i}}^{n+1} + B_p(\mathbf{U}_{\mathbf{i}}^{n+1},\mathbf{g}_{\mathbf{i}}^{n+1}), && i=0,j=0,1,\dots,N, && (17)
\end{aligned}
$$

where the boundary forcing satisfies

$$
B_p(\mathbf{U},\mathbf{g}) = -\frac{\partial g^u}{\partial t} - g^u D_{0x}U - g^v D_{0y}g^v + \nu D_{+y}D_{-y}g^u .
$$

To improve the stability properties of the time-integrator, we often use the above scheme as the predictor followed by a second-order Adams-Moulton corrector.

1.2 A semi-implicit scheme

As another example, we have implemented a semi-implicit method that combines a Crank-Nicholson treatment for the viscous terms and an Adams-Bashforth approach for the advection terms and pressure. Instead of equation (12) we use

$$\frac{\mathbf{U}_{\mathbf{i}}^{n+1}-\mathbf{U}_{\mathbf{i}}^{n}}{\Delta t}=\frac{3}{2}(L_E\mathbf{U}_{\mathbf{i}}^{n}+\mathbf{F}_{\mathbf{i}}^{n})-\frac{1}{2}(L_E\mathbf{U}_{\mathbf{i}}^{n-1}+\mathbf{F}_{\mathbf{i}}^{n-1})+\frac{1}{2}(L_I\mathbf{U}_{\mathbf{i}}^{n+1}+L_I\mathbf{U}_{\mathbf{i}}^{n})$$

together with equations (13-15) to advance the velocity in time. Again, we can improve the stability properties by using the above scheme as the predictor followed by a second order Adams-Moulton corrector.

Since the boundary condition for the pressure (17) depends on ν/h^2 and since the pressure is taken explicitly in the time stepping scheme, one might suspect that Δt must depend on the ratio h^2/ν. This is indeed the case when a discrete version of (9) is used as the boundary condition for the pressure. For implicit time stepping, a more stable pressure boundary condition is formed by explicitly removing the dilatation on the boundary in the highest order term, $\Delta\mathbf{u}$, by using the vector identity

$$\Delta\mathbf{u}=\nabla(\nabla\cdot\mathbf{u})-\nabla\times\nabla\times\mathbf{u},$$

together with $\nabla(\nabla\cdot\mathbf{u})=0$, to give

$$\frac{\partial p}{\partial n}=\mathbf{n}\cdot\left(-\mathbf{g}_t-(\mathbf{g}\cdot\nabla\mathbf{u})-\nu\nabla\times\nabla\times\mathbf{u}\right). \tag{18}$$

We call this the curl-curl boundary condition for the pressure. This boundary condition was apparently first advocated by Karniadakis, Israeli and Orszag [14] as the appropriate boundary condition for the pressure. Unlike equation (9) this new equation does add new information to the system and can be used as an alternative boundary condition to $\nabla\cdot\mathbf{u}=0$. Note that the boundary condition (18) is specifying the normal derivative of the dilatation to be zero on the boundary since (18) was derived from (9) using

$$\frac{\partial}{\partial n}(\nabla\cdot\mathbf{u})=0. \tag{19}$$

Referring back to equation (3) we see that the above boundary condition, together with the initial condition $\delta(\mathbf{x},0)=0$, will also force the dilatation to be zero for all time.

On the square grid $\mathbf{G}$, the discrete version of (18) becomes

$$D_{0x}P_{\mathbf{i}}^{n+1}=-\nu D_{0x}D_{0y}V_{\mathbf{i}}^{n+1}+B_p(\mathbf{U}_{\mathbf{i}}^{n+1},\mathbf{g}_{\mathbf{i}}^{n+1}),\quad i=0,j=0,1,\dots,N, \tag{20}$$

Note that the stencil for the viscous term is significantly different in the discretized curl-curl (20) and div-grad (17) pressure boundary conditions; this is the source of the different stability properties of the two boundary conditions. A detailed stability analysis, Petersson [20], shows that the time step is only determined by the advection terms (i.e. is independent of ν) if (17) is replaced by the curl-curl boundary condition (20). This is somewhat remarkable, since the pressure is treated explicitly.

We remark that in our implementation, we use the curl-curl pressure boundary condition both for the explicit and semi-implicit schemes.

It is straight-forward to build time stepping schemes that are accurate to any desired order in time. The reason for this is that in the approach we have taken we have effectively reduced the solution of the incompressible Navier-Stokes equations to solving a system of ODE's for $\mathbf{U_i}$:

$$\frac{d}{dt}\mathbf{U_i} = \mathbf{F}(\mathbf{U_i}, t),$$

since we can treat the pressure simply as a function of the velocity.

The difference approximations presented here can be easily extended to curvilinear grids and to composite overlapping grids. The approximations can be also be made fourth order accurate in space, see [10] for further details.

1.3 The compatibility condition for the pressure equation

If the pressure has a Neumann boundary condition on all boundaries the pressure equation will be singular and it is only solvable if the right hand side satisfies a compatibility condition on the velocity. In order to solve this singular system one could, for example, eliminate one equation and replace it with an equation that, for example, sets the value of p at a point or sets the mean value for p. Rather than single out a particular equation to be removed we prefer to use a different approach which is better conditioned. If we denote the equation for the pressure as the matrix equation,

$$Ax = b$$

then we solve the augmented system

$$\begin{bmatrix} A & r \\ r^T & 0 \end{bmatrix} \begin{bmatrix} x \\ \beta \end{bmatrix} = \begin{bmatrix} b \\ 0 \end{bmatrix}.$$

Here r is the right null vector of A; the vector with all components equal to one. It is well-known that this augmented system is non-singular and has an unique solution. The last equation will set the mean value of p to zero.

1.4 The discrete divergence

In practice it is important to include the divergence damping term, $\alpha_{\mathbf{i}}\ \nabla_h \cdot \mathbf{U_i}$, in the pressure equation (6). Alternatively, one could apply an extra explicit projection to the solution after every step, but this would require a significant amount of extra work. The damping coefficient $\alpha(\mathbf{x},t)$ can be chosen to be quite large. When using an explicit time stepping approach, we choose

$$\alpha = C_d \ \frac{\nu}{h^2},$$

where the coefficient C_d is usually taken to be about one. On a rectangular grid this makes α proportional to $1/\Delta t$. Note that on a curvilinear grid the coefficient will vary in space. One might wonder whether this divergence damping term, which is a potentially order one addition to the pressure equation, will destroy the accuracy of the method. In [12] we analyse this damping term using normal-mode stability analysis and show that the method retains it's accuracy even with this term. In practice we find that increasing C_d will result in a decrease of the maximum dilatation (up to a point) but it can also increase the error in the pressure.

A von Neumann stability analysis shows that the allowable time step, Δt, will depend on the size of α. For implicit methods we do not want the damping coefficient to significantly reduce the time step so it is necessary to limit the size of α by $C/\Delta t$ for a constant $C = O(1)$.

2 Numerical results

In this section we present some results from a numerical implementation of the scheme described in this paper. The method was implemented in the **OverBlown** flow solver. **OverBlown** is developed using the **Overture** object-oriented framework and can solve the incompressible Navier-Stokes equations on composite overlapping grids in two and three space dimensions. Both **OverBlown** and **Overture** are freely available from the internet at `http://www.llnl.gov/-casc/Overture`. Currently **OverBlown** only has a second-order accurate spatial approximation implemented, although a fourth-order accurate method has previously been developed in Fortran [10]. Details on the discretization and solution procedure, as well as more extensive convergence studies can be found in [11].

As a first test we use the method of analytic solutions to define the following exact solution to the (forced) two-dimensional incompressible Navier-Stokes equations,

$$\begin{aligned}
u_{\text{true}}(x,y,t) &= (x^2+2xy+y^2)\ T(t),\\
v_{\text{true}}(x,y,t) &= (x^2-2xy-y^2)\ T(t),\\
p_{\text{true}}(x,y,t) &= (x^2+\frac{1}{2}xy+y^2-1)\ T(t),\\
T(t) &= 1+\frac{1}{2}t+\frac{1}{3}t^2.
\end{aligned}$$

The exact solution has been chosen to be divergence free to simplify the implementation. This test example is extremely useful for our purposes since this

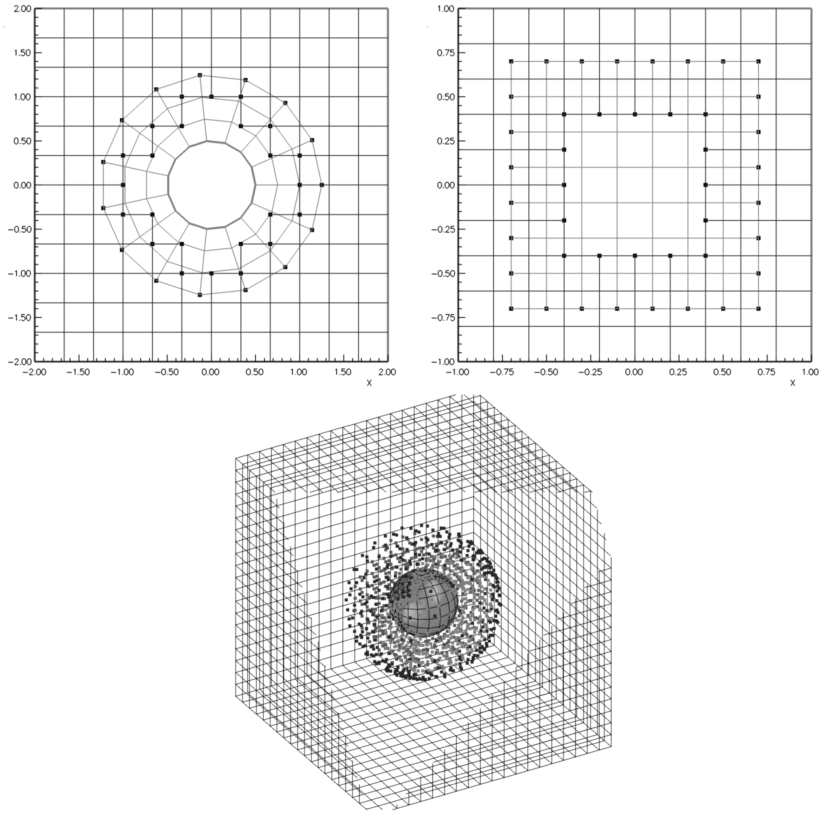

Fig. 3. Grids used for the convergence studies: circle-in-a-channel (top-left), square-in-a-square (top right), sphere-in-a-box (bottom left)

solution should also be an *exact solution to the discrete equations* on a rectangular grid. Indeed the errors obtained when solving this problem are of the order of the round-off error for grids consisting of a single square and also for a composite grid consisting of a rotated square in a square, as shown in Table 1. For debugging purposes this is an excellent test since, modulo roundoff errors, the numerical errors should be exactly zero at every time step. For these grids, it is therefore not necessary to run extensive convergence tests using grid refinement to check convergence rates.

Table 1. Maximum errors when the analytic solution is a quadratic polynomial, $\nu = .1$, $t = 1.0$. Since the grids are rectangular the method gives the exact answer to within roundoff. The grid "sis" is the square-in-a-square overlapping grid consisting of a square embedded in a larger square shown in figure (3). The 3D grid "rbib" is a rotated box within a box.

grid	method	$\|p - p_e\|_\infty$	$\|u - u_e\|_\infty$	$\|v - v_e\|_\infty$	$\|w - w_e\|_\infty$	$\|\nabla \cdot \mathbf{u}\|_\infty$
square10	explicit	$3.1\ 10^{-15}$	$1.8\ 10^{-15}$	$8.9\ 10^{-16}$		$6.2\ 10^{-15}$
square10	implicit	$1.2\ 10^{-14}$	$9.8\ 10^{-15}$	$3.8\ 10^{-15}$		$5.0\ 10^{-14}$
sis	explicit	$1.3\ 10^{-14}$	$3.6\ 10^{-15}$	$3.2\ 10^{-15}$		$1.2\ 10^{-14}$
box10	explicit	$1.8\ 10^{-14}$	$2.7\ 10^{-15}$	$1.6\ 10^{-15}$	$1.8\ 10^{-15}$	$1.6\ 10^{-14}$
rbib	explicit	$1.3\ 10^{-10}$	$6.4\ 10^{-12}$	$8.2\ 10^{-12}$	$1.2\ 10^{-11}$	$1.1\ 10^{-11}$

In three dimensions we use the exact solution

$$\begin{aligned}
u_{\text{true}}(x, y, t) &= (x^2 + 2xy + y^2 + xz)\ T(t), \\
v_{\text{true}}(x, y, t) &= (x^2 - 2xy - y^2 + 3xz)\ T(t), \\
w_{\text{true}}(x, y, t) &= (x^2 + y^2 - 2z^2)\ T(t), \\
p_{\text{true}}(x, y, t) &= (x^2 + \frac{1}{2}xy + y^2 + z^2 - 1)\ T(t),
\end{aligned}$$

with results shown in Table 1 for a box (`box10`) and a rotated-box in a box (`rbib`).

On curvilinear grids, the above polynomial functions are not exact solutions to the discrete equations due to the variable coefficients in the metric terms. Here the order of accuracy can be checked by performing a grid refinement study, see Tables 2-3. In these runs, the convergence rates were estimated by least squares fits to the data.

The discrete pressure equation has an additional divergence damping term, $\alpha\nabla \cdot \mathbf{u}$. To illustrate the effect this term has on the solution we present some convergence studies. We force the equations so that the exact solution is known. In two space dimensions we use

$$\begin{aligned}
\mathbf{u}_{\text{true}}(x, y, t) &= \Big(\ \sin^2(fx)\sin(2fy)\cos(2\pi t)\ ,\ \ -\sin(2fx)\sin^2(fy)\cos(2\pi t)\ \Big), \\
p_{\text{true}}(x, y, t) &= \sin(fx)\sin(fy)\cos(2\pi t).
\end{aligned}$$

We solve the IBVP with and without the damping term turned on. The domain is taken to be the unit square with all boundaries being walls where the velocity is specified. The results for the fourth-order method are given in Tables 4 and 5, where the maximum errors in $\mathbf{u}$, p and $\nabla \cdot \mathbf{u}$ are reported. The estimated convergence rate σ, error $\propto h^\sigma$, is also shown. Here, σ is estimated by a least squares fit to the maximum errors given in the table.

The results show that although the methods are converging at the expected rates without the damping term, the errors are significantly reduced when damping term is used.

2.1 Remarks on the pressure boundary condition

To illustrate the benefits of using the curl-curl boundary condition (18) we compare the numerically determined largest stable time-step to that of the div-grad boundary condition (9), for the semi-implicit time-stepping scheme described in Section 1.2. The results are presented in Table 6. The grid is a circle-in-a-channel and the Reynolds number based on the diameter of the circular cylinder is $Re = 100$. Note that the allowable time step for the curl-curl boundary condition is independent of ν/h^2 so that Δt only depends on the advection terms (which are treated explicitly). In contrast, the div-grad boundary condition (9) requires a significantly smaller Δt that depends on ν/h^2.

In practice, it is not uncommon for application codes to use the simpler pressure boundary condition

$$\frac{\partial p}{\partial n} = 0. \tag{21}$$

Using this boundary condition, it is not difficult to attain a stable scheme; a likely reason for the popularity of the approach. On the other hand, a naïve implementation of the accurate condition $\partial p/\partial n = \nu \mathbf{n} \cdot \Delta \mathbf{u}$ can easily lead to an unstable method. For high-Reynolds number laminar boundary layer flow, equation (21) could be a good approximation since $\partial p/\partial n = O(Re^{-1/2})$ tends to zero as $Re \to \infty$. To evaluate this approximation at a finite Reynolds number, we computed the unsteady flow around two circular cylinders in a channel using both the curl-curl pressure boundary condition and (21). In this case, $Re = 10^3$ based on the diameter of one cylinder. As can be seen in Figure 4, the flow

Table 2. Maximum errors at $t = .5$ for a polynomial analytic solution with $\nu = .1$. The domain is discretized by the circle-in-a-channel grid shown in figure (3) where the coarsest grid ($g = 1$) has $13 \times 13 \bigcup 16 \times 3$ grid points. The time stepping was a second-order explicit predictor corrector method. The column entitled h_1/h_g denotes the ratio of the grid spacing on grid 1 to the spacing on grid g.

grid	h_1/h_g	$\|p - p_e\|_\infty$	$\|u - u_e\|_\infty$	$\|v - v_e\|_\infty$	$\|\nabla \cdot \mathbf{u}\|_\infty$
$g = 1$	1	$3.3\ 10^{0}$	$2.8\ 10^{-1}$	$4.0\ 10^{-1}$	$6.5\ 10^{-1}$
$g = 2$	2	$3.0\ 10^{-1}$	$4.2\ 10^{-2}$	$4.4\ 10^{-2}$	$1.5\ 10^{-1}$
$g = 3$	4	$6.0\ 10^{-2}$	$1.0\ 10^{-2}$	$8.2\ 10^{-3}$	$3.5\ 10^{-2}$
$g = 4$	8	$7.0\ 10^{-3}$	$2.2\ 10^{-3}$	$1.4\ 10^{-3}$	$9.8\ 10^{-3}$
rate		2.9	2.3	2.7	2.0

Table 3. Maximum errors at $t = .1$ for a polynomial analytic solution with $\nu = .1$. The grid is a sphere-in-a-box. The coarse grid, g=1, consists of component grids with $17\times17\times17 \bigcup 12\times12\times4 \bigcup 12\times12\times4$ grid points. The column entitled h_1/h_g denotes the ratio of the grid spacing on grid 1 to the spacing on grid g.

grid	h_1/h_g	$\|p-p_e\|_\infty$	$\|u-u_e\|_\infty$	$\|v-v_e\|_\infty$	$\|w-w_e\|_\infty$	$\|\nabla\cdot\mathbf{u}\|_\infty$
$g=1$	1	2.4×10^{0}	8.3×10^{-2}	7.1×10^{-2}	8.5×10^{-2}	6.0×10^{-1}
$g=2$	2	6.4×10^{-1}	2.6×10^{-2}	1.9×10^{-2}	2.0×10^{-2}	1.6×10^{-1}
$g=3$	3	2.6×10^{-1}	1.1×10^{-2}	7.7×10^{-3}	7.6×10^{-3}	7.8×10^{-2}
rate		2.0	1.8	2.0	2.2	1.9

Table 4. Maximum errors at $t = 1.$ with the 4th order spatial approximation and $\nu = .05$. The divergence damping coefficient is $C_d = 1$. Compare these results to Table 5 where no divergence damping is used.

grid	$\|\mathbf{u}-\mathbf{u}_e\|_\infty$	$\|p-p_e\|_\infty$	$\|\nabla\cdot\mathbf{u}\|_\infty$
20×20	$9.3\ 10^{-4}$	$8.0\ 10^{-3}$	$2.2\ 10^{-2}$
30×30	$1.2\ 10^{-4}$	$1.4\ 10^{-3}$	$2.4\ 10^{-3}$
40×40	$2.8\ 10^{-5}$	$4.3\ 10^{-4}$	$5.1\ 10^{-4}$
rate	5.0	4.2	5.4

Table 5. Maximum errors at $t = 1.$ with the 4th order spatial approximation and $\nu = .05$. The divergence damping coefficient is $C_d = 0$. Compare these results to Table 4 where divergence damping is used.

grid	$\|\mathbf{u}-\mathbf{u}_e\|_\infty$	$\|p-p_e\|_\infty$	$\|\nabla\cdot\mathbf{u}\|_\infty$
20×20	$2.4\ 10^{-3}$	$1.3\ 10^{-2}$	$6.4\ 10^{-2}$
30×30	$5.1\ 10^{-4}$	$2.5\ 10^{-3}$	$1.3\ 10^{-2}$
40×40	$1.7\ 10^{-4}$	$8.2\ 10^{-4}$	$4.4\ 10^{-3}$
rate	3.8	4.0	3.9

is laminar on the leading sides and detached on the trailing sides of the cylinders. The pressure on the boundary of the upper cylinder using both pressure boundary conditions is presented in Figure 5. Clearly, the simplified pressure boundary condition (21) leads to an inaccurate boundary pressure. To validate the computational results, we use the laminar boundary layer results provided by Schlichting [21], pp.170–173, for 2–d flow around a circular cylinder. Schlichting

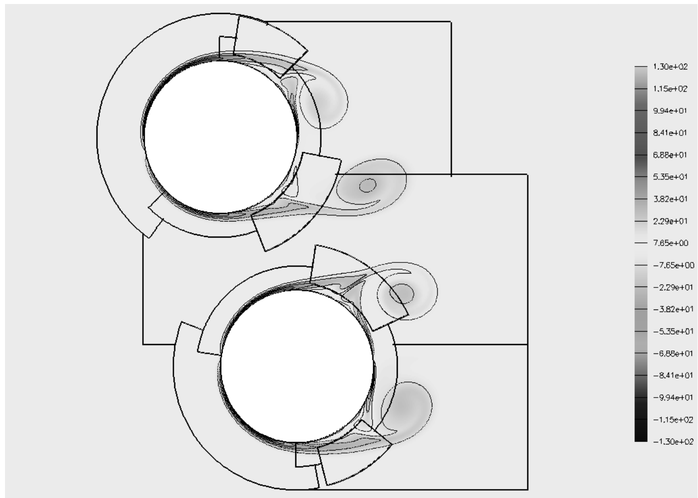

Fig. 4. The vorticity around two circular cylinders in a channel at time $t = 2$ plotted with 18 equally spaced contour lines between ± 130. The Reynolds number based on the diameter of one cylinder is $Re = 10^3$.

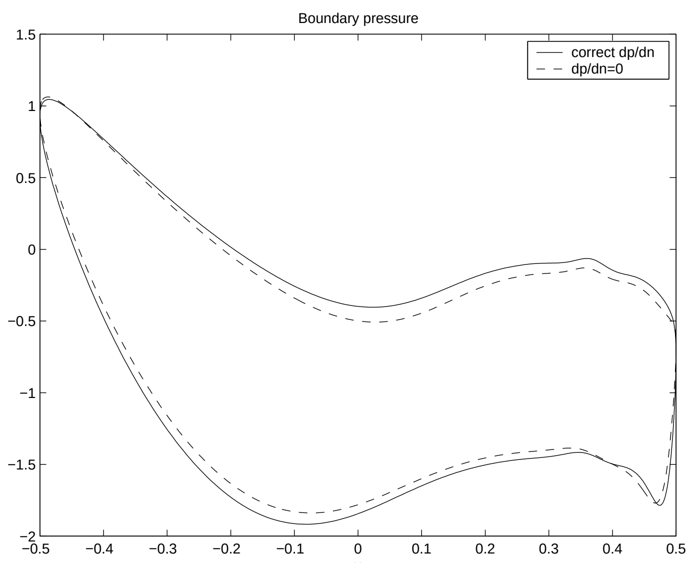

Fig. 5. The (kinematic) pressure on the boundary of the upper cylinder using the curl-curl pressure boundary condition (solid) and the simple boundary condition (21) (dashed) at time $t = 2$. The Reynolds number is $Re = 10^3$. Note that the inflow velocity $U_{in} = 1$ in this computation, so the pressure coefficient $C_p = 2p/U_{in}^2$, equals twice the kinematic pressure p.

Table 6. A comparison of the div-grad boundary condition (9) and the curl-curl boundary condition (18) for semi-implicit time-stepping. Shown are the largest stable time-steps and maximum errors for a forced computation. The time-step for the curl-curl boundary condition can be chosen much larger since it is does not depend on the ratio ν/h^2. The coarse grid had $41 \times 21 \cup 21 \times 14$ points and the fine grid had $81 \times 41 \cup 41 \times 27$ points.

BC	Grid	Δt	$\|p - p_e\|_\infty$	$\|u - u_e\|_\infty$	$\|v - v_e\|_\infty$	$\|\nabla \cdot \mathbf{u}\|_\infty$
div-grad	coarse	$2.0 \cdot 10^{-3}$	$5.8 \cdot 10^{-2}$	$4.2 \cdot 10^{-2}$	$8.6 \cdot 10^{-2}$	$1.1 \cdot 10^{-1}$
div-grad	fine	$5.0 \cdot 10^{-4}$	$5.7 \cdot 10^{-3}$	$8.8 \cdot 10^{-3}$	$1.5 \cdot 10^{-2}$	$2.4 \cdot 10^{-2}$
curl-curl	coarse	$1.1 \cdot 10^{-2}$	$5.8 \cdot 10^{-2}$	$4.2 \cdot 10^{-2}$	$8.6 \cdot 10^{-2}$	$1.1 \cdot 10^{-1}$
curl-curl	fine	$5.5 \cdot 10^{-3}$	$5.8 \cdot 10^{-3}$	$8.8 \cdot 10^{-3}$	$1.5 \cdot 10^{-2}$	$2.4 \cdot 10^{-2}$

provides a graph for the boundary shear stress,

$$\tau_0 = \mu \frac{\partial u^{(s)}}{\partial n},$$

along the leading side of the cylinder. (Here, $u^{(s)}$ denotes the tangential velocity component and μ is the dynamic viscosity.) By evaluating the slope of that graph, we obtain $\partial^2 u^{(s)}/\partial s \partial n$, where s is the arclength along the boundary of the cylinder. This term is proportional to the normal derivative of the pressure, since

$$\frac{\partial p}{\partial n} = -\nu \mathbf{n} \cdot \nabla \times \nabla \times \mathbf{u} = -\nu \frac{\partial^2 u^{(s)}}{\partial s \partial n}. \tag{22}$$

In Figure 6, we plot (22) for $Re = 10^3$. At this Reynolds number, the normal derivative of the pressure is not small even in the laminar region on the leading side of the cylinder. On the trailing side of the cylinder, where the flow is detached, the normal derivative is of the order $O(1)$. We believe this will be the case also for higher Reynolds numbers, since the assumptions of laminar boundary layer theory do not apply for detached flows. We conclude that it is important to use one of the accurate boundary conditions (9) or (18) for laminar flows at low and medium Reynolds numbers as well as detached flows at any Reynolds number.

As an illustration of some more advanced applications of our approach, in Figure 1 we show the solution to an incompressible flow containing two rigid cylinders. The cylinders fall under the influence of gravity and their motion is determined by the forces exerted by the fluid. In this computation, the overlapping grids are recomputed at every time step. Figure 2 shows the flow past a rotating disk and Figure 7 shows the flow past a valve.

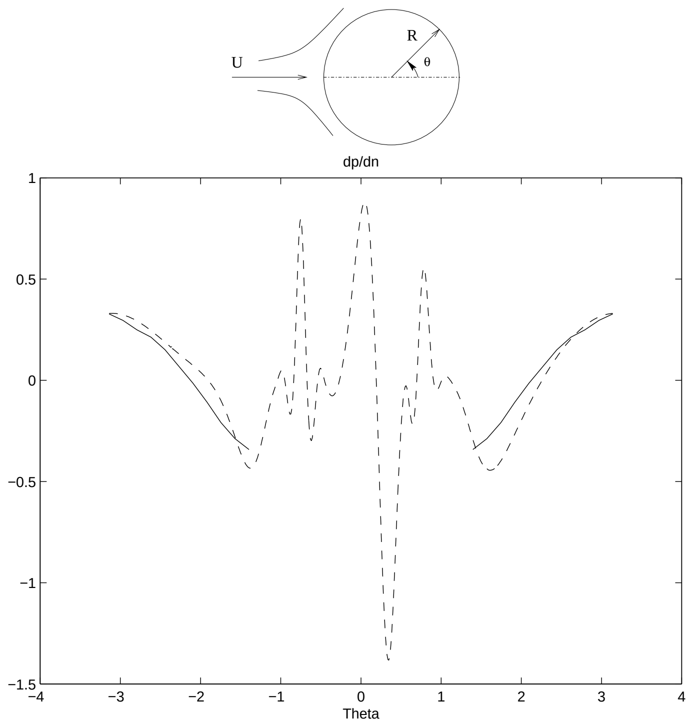

Fig. 6. The normal derivative of the pressure along the boundary of the circular cylinder for $Re \equiv 2UR/\nu = 10^3$. The solid line was evaluated from the slope of the boundary shear stress for a single cylinder, provided by Schlichting [21]. The dashed line was calculated along the upper cylinder in the flow shown in Figure 4.

3 Software availability

The **OverBlown** flow solver and **Overture** are freely available from the internet at `http://www.llnl.gov/casc/Overture`.

Acknowledgments: The authors thank Heinz-Otto Kreiss for many interesting discussions on the present subject.

This work was performed under the auspices of the U.S. Department of Energy by the University of California, Lawrence Livermore National Laboratory under contract No. W-7405-Eng-48.

References

1. S. Abdallah, *Numerical solutions for the pressure poisson equation with Neumann boundary conditions using a non-staggered grid, I*, J. Comp. Phys., 70 (1987), pp. 182–192.

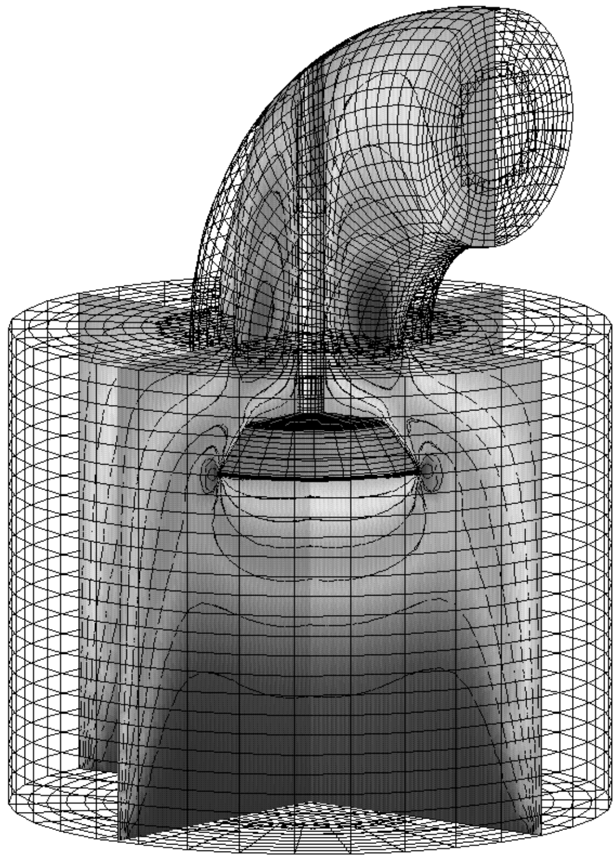

Fig. 7. Flow past a valve.

2. J. B. Bell, P. Colella, and H. M. Glaz, *A second-order projection method for the incompressible Navier-Stokes equations*, J. Comp. Phys., 85 (1989), pp. 257–283.
3. D. L. Brown, R. Cortez, and M. L. Minion, *Accurate projection methods for the incompressible Navier–Stokes equations*, J. Comp. Phys., 168 (2001), pp. 464–499.
4. A. J. Chorin, *A numerical method for solving incompressible viscous flow problems*, J. Comp. Phys., 2 (1967), pp. 12–26.
5. ——, *Numerical solution of the Navier-Stokes equations*, Math. Comp., 22 (1968), pp. 745–762.
6. W. E and J. Guo Liu, *Projection method II: Godunov-Ryabenki analysis*, SIAM J. of Numer. Anal., 33 (1996), pp. 1597–1621.
7. P. M. Gresho and R. L. Sani, *On the pressure boundary conditions for the incompressible Navier-Stokes equations*, International Journal for Numerical Methods in Fluids, 7 (1987), pp. 1111–1145.

8. F. Harlow and J. Welch, *Numerical calculation of time-dependent viscous incompressible flow of fluid with free surface*, J. Comp. Phys., 8 (1965), pp. 2182–2189.
9. W. Heinrichs, *Splitting techniques for the unsteady Stokes equations*, SIAM J. of Numer. Anal., 35 (1998), pp. 1646–1662.
10. W. Henshaw, *A fourth-order accurate method for the incompressible Navier-Stokes equations on overlapping grids*, J. Comp. Phys., 113 (1994), pp. 13–25.
11. ———, *OverBlown: A fluid flow solver for overlapping grids, user guide*, Research Report UCRL-MA-134288, Lawrence Livermore National Laboratory, 1999.
12. W. Henshaw and H.-O. Kreiss, *Analysis of a difference approximation for the incompressible Navier-Stokes equations*, Research Report LA-UR-95-3536, Los Alamos National Laboratory, 1995.
13. W. Henshaw, H.-O. Kreiss, and L. Reyna, *A fourth-order accurate difference approximation for the incompressible Navier-Stokes equations*, Comput. Fluids, 23 (1994), pp. 575–593.
14. G. Karniadakis, M. Israeli, and S. A. Orszag, *High-order splitting methods for the incompressible Navier-Stokes equations*, J. Comp. Phys., 97 (1991), pp. 414–443.
15. J. Kim and P. Moin, *Application of a fractional-step method to incompressible Navier-Stokes equations*, J. Comp. Phys., 59 (1985), pp. 308–323.
16. C. Kiris, D. Kwak, S. Rogers, and I. Chang, *Computational approach for probing the flow through artificial heart devices*, ASME J. of Biofluidmechanical Engineering, 119 (1997), pp. 452–460.
17. K. Korczak and A. T. Patera, *An isoparametric spectral element method for solution of the Navier-Stokes equations in complex geometry*, J. Comp. Phys., 62 (1986), pp. 361–382.
18. S. A. Orszag, M. Israeli, and M. O. Deville, *Boundary conditions for incompressible flows*, J. Sci. Comp., 1 (1986), pp. 75–111.
19. J. B. Perot, *An analysis of the fractional step method*, J. Comput. Phys., 108 (1993), pp. 51–58.
20. N. A. Petersson, *Stability of pressure boundary conditions for Stokes and Navier-Stokes equations*, J. Comp. Phys., 172 (2001), pp. 40–70.
21. H. Schlichting, *Boundary-Layer Theory*, McGraw-Hill, New York, 1979. Seventh Edition.
22. J. Shen, *On error estimates of the projection methods for the Navier-Stokes equations: second-order schemes*, Math. Comp., 65 (1996), pp. 1039–1065.
23. J. Strikwerda, *Finite difference methods for the Stokes and Navier-Stokes equations*, SIAM J. Sci. Stat. Comput., 5 (1984), pp. 56–68.
24. J. C. Strikwerda and Y. S. Lee, *The accuracy of the fractional step method*, SIAM J. Numer. Anal., 37 (1999), pp. 37–47.
25. R. Temam, *Sur l'approximation de la solution des equation de Navier-Stokes par la méthode des fractionnarires II*, Arch. Rational Mech. Anal., 33 (1969), pp. 377–385.
26. J. A. Wright and W. Shyy, *A pressure-based composite grid method for the Navier-Stokes equations*, J. Comp. Phys., 107 (1993), pp. 225–238.